GDCh

Communications

Angewandte
Chemie
International Edition
www.angewandte.org

Exploiting Cooperative Catalysis for the On-Surface Synthesis of Linear Heteroaromatic Polymers via Selective C–H Activation

Xunshan Liu[+], Adam Matej[+], Tim Kratky, Jesús I. Mendieta-Moreno, Sebastian Günther, Pingo Mutombo, Silvio Decurtins, Ulrich Aschauer, Jascha Repp, Pavel Jelinek,* Shi-Xia Liu,* and Laerte L. Patera*

Abstract: *Regiospecific C–H activation is a promising approach to achieve extended polymers with tailored structures. While a recent on-surface synthetic approach has enabled regioselective homocoupling of heteroaromatic molecules, only small oligomers have been achieved. Herein, selective C–H activation for dehydrogenative C–C couplings of hexaazatriphenylene by Scholl reaction is reported for the first time. By combining low-temperature scanning tunneling microscopy (STM) and atomic force microscopy (AFM), we revealed the formation of one-dimensional polymers with a double-chain structure. The details of the growth process are rationalized by density functional theory (DFT) calculations, pointing out a cooperative catalytic action of Na and Ag adatoms in steering the C–H selectivity for the polymerization.*

The dehydrogenative coupling reaction of two arene rings and the ring-closing cyclodehydrogenation process mediated by non-oxidizing Lewis acids (Scholl reaction) as well as the analogous oxidative aromatic coupling reaction occupy a prominent place in the synthetic chemistry of polycyclic (hetero)aromatic compounds.[1–4] These synthetic protocols are particularly advantageous since biaryl linkages can be formed without any prefunctionalization of precursor molecules. Not surprisingly, the Scholl reaction proved to be most useful for the formation of multiple fused rings to obtain polycyclic arenes and nanographene compounds.[5–9] However, the C–H activation/arylation step in the synthesis of polycyclic aromatic hydrocarbons (PAHs) generally lacks selectivity because the C–H bonds have, besides a low intrinsic reactivity, only small relative differences in their reactivity.[9,10] Complementary to the well-established Scholl reaction in solution, the analogous surface-assisted C–C coupling process exhibits stunning efficiency for the fabrication of nanographenic and other atomic-scale structures.[11–13] For the intramolecular bond formation, the cyclodehydrogenation process occurs between two arene rings in close proximity and consequently, its regioselectivity can to a large extent be controlled.[12,14–16] However, for the intermolecular case, the bond selectivity of the dehydrogenative aryl–aryl coupling cannot be predicted a priori when the molecules contain several C–H bonds.[17–19]

Recently, the selectivity in aryl–aryl coupling has been addressed by exploiting the regioselectivity of on-surface homocoupling of tetraazapolycyclic pyrazino[2,3-*f*:4,7]phenanthroline molecules (pap) on the Au(111) substrate.[20] There the C–H bond scission was reported to be clearly regiospecific, since *ortho*-hydrogen atoms of the pyrazine rings are preferentially activated over their pyridine equivalents, as clarified by scanning tunneling (STM) and noncontact atomic force microscopy (AFM)

---

[*] Dr. X. Liu,[+] Prof. Dr. S. Decurtins, Prof. Dr. U. Aschauer,
PD Dr. S.-X. Liu
Department of Chemistry, Biochemistry and Pharmaceutical Sciences
University of Bern
3012 Bern (Switzerland)
E-mail: shi-xia.liu@unibe.ch

Dr. X. Liu[+]
Department of Chemistry, Zhejiang Sci-Tech University
Hangzhou (China)

A. Matej,[+] Dr. J. I. Mendieta-Moreno, Dr. P. Mutombo,
Prof. Dr. P. Jelinek
Institute of Physics of Czech Academy of Sciences
16200 Prague (Czech Republic)
E-mail: jelinekp@fzu.cz

A. Matej,[+] Prof. Dr. P. Jelinek
Regional Centre of Advanced Technologies and Materials
Czech Advanced Technology and Research Institute (CATRIN)
Palacký University Olomouc
78371 Olomouc (Czech Republic)

T. Kratky, Prof. Dr. S. Günther, Dr. L. L. Patera
Department of Chemistry and Catalysis Research Center
Technical University of Munich
85748 Garching (Germany)
E-mail: laerte.patera@tum.de

Prof. Dr. J. Repp, Dr. L. L. Patera
Institute of Experimental and Applied Physics
University of Regensburg
93053 Regensburg (Germany)

[+] These authors contributed equally to this work.

imaging.[20] However, the resulting covalent structures were limited in size, being restricted to small clusters, mainly composed of dimers, trimers and tetramers. While this approach allows controlling the selectivity of the Scholl reaction, novel strategies for the synthesis of extended polymers are still needed. Cooperative catalysis, where multiple catalysts and catalytic cycles work synergistically to promote single-bond formation, is an appealing approach to achieve new reaction schemes.[21–23] However, its potential in the field of on-surface synthesis has largely been unexplored.

Here, we report on a surface-assisted synthetic protocol which leads to selective C–H activation for dehydrogenative C–C couplings of hexaazatriphenylene (HAT) molecules,[24] affording linear heteroaromatic polymers in the presence of Na adatoms on a Ag(111) surface (Scheme 1). Each HAT chain is featured with contiguous bidentate N^N coordination pockets induced by cisoid conformations for catena-2,2′-(1,10-phenanthroline) skeletons along the chain. Two chains are aligned in parallel through Na coordination to N^N chelating pockets. Previously, gold–adatom coordination to a tetradentate N^N pocket was observed to steer a cisoid conformation for the formation of a dimeric pap molecule, two of which are also parallel aligned via two gold adatoms coordination to N^N pockets.[20] Similarly, a cisoid on-surface conformation of 2,2′-bipyridine triggered by metal coordination was demonstrated.[25] Notably, its chelate complex with a single Na atom is formed when a π-conjugated tetrathiafulvalene-fused dipyridophenazine molecule is adsorbed on NaCl/Cu(111).[26] In the present work, the growth of two coordinatively bonded HAT chains, which are observed to be of equal length, is inherently due to a regiospecific homocoupling of a (HAT)$_2$-Na dimer through selective activation of the C–H bonds in *meta*-positions to the N^N chelating pocket. In other words, this polymerization is initiated by complexation with Na forming a (HAT)$_2$-Na dimer while the subsequent C–H activation with high selectivity is catalyzed by individual Ag adatoms, finally leading to a double-chain structure via the dehydrogenative aryl-aryl coupling.

Deposition of the HAT molecules on the Ag(111) surface kept at ≈10 K and sequential annealing to 300 K (Figure 1a) result in extended crystals, consisting mainly of
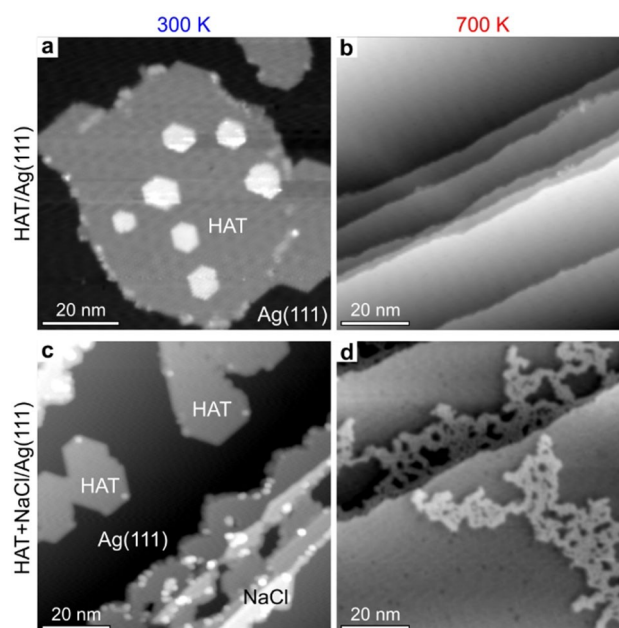

Figure 1. On-surface synthesis of heteroaromatic polymers. a, b) STM images acquired after annealing a sub-monolayer of HAT on Ag(111) to 300 K (a), showing extended self-assembled monolayers, with small bilayer islands, and to 700 K (b). c, d) STM images acquired after annealing a sub-monolayer of HAT and NaCl (0.3 ML) on Ag(111) to 300 K (c) and 700 K (d). All the images have been acquired in constant-current STM mode. a) Measurement parameters: tunneling current $I = 1.7$ pA, sample bias voltage $V = 1.0$ V. b) $I = 1.9$ pA, $V = 1.0$ V. c) $I = 1.4$ pA, $V = 1.5$ V. d) $I = 1.1$ pA, $V = 1.0$ V.

self-assembled monolayer islands.[24] Subsequent annealing to 700 K leads to the complete desorption of the molecules (Figure 1b). A different scenario is instead observed once a NaCl sub-monolayer (ML) is co-deposited together with the HAT molecules (Figure 1c). There, upon subsequent annealing to 700 K, no NaCl island has been observed, while polymers are found on the Ag surface (Figure 1d), covering the step edges, and extending on the flat terraces. A close-up at the polymers by STM imaging (Figure 2a) shows that the products are composed of linear structures (see Figure S1).
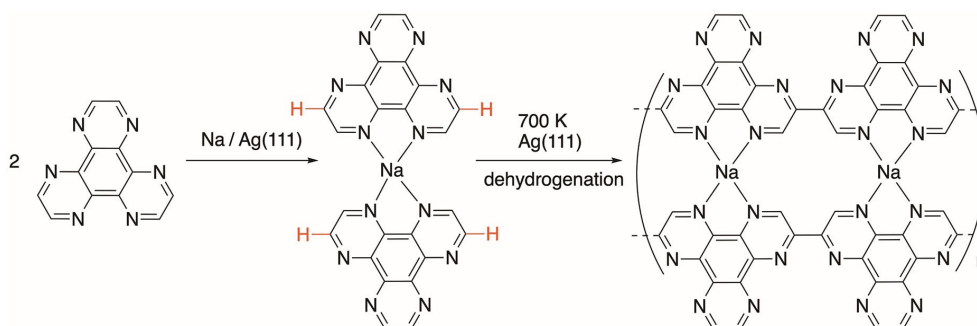
Scheme 1. A schematic illustration of the surface-assisted polymerization of HAT molecules in the presence of Na. Adjacent chains are aligned via contiguous N∧N coordination pockets offering four-fold coordination sites.
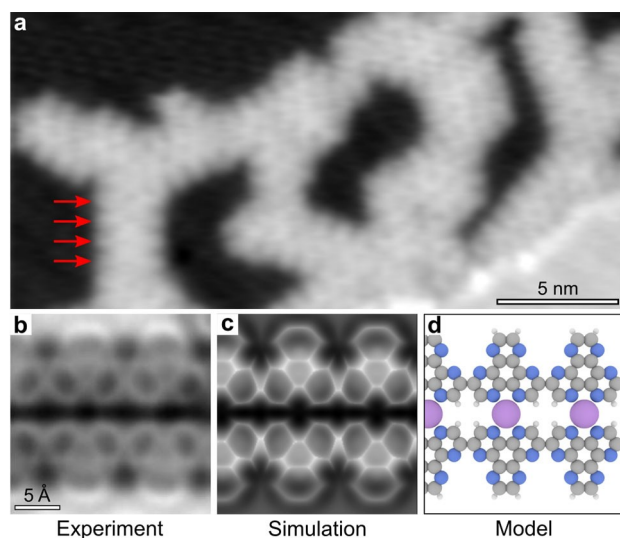
Figure 2. Linear heteroaromatic polymers. a) Constant-current STM image after annealing to 700 K of a Ag(111) surface covered by a sub-monolayer of HAT and NaCl (0.3 ML). Arrows indicate the positions of monomers in a linear chain ($I=1.3$ pA, $V=1.0$ V). b) Constant-height Δf AFM image acquired with a CO-functionalized tip at $\Delta z=-2.7$ Å, given with respect to an STM setpoint of ($I=1.1$ pA, $V=0.1$ V). AFM oscillation amplitude, $A=0.5$ Å. c, d) Simulated AFM image and structural model, respectively. d) Grey, blue, white and violet spheres represent carbon, nitrogen, hydrogen and sodium atoms, respectively.

These experimental observations raise the point about the role of the co-deposited NaCl film in enabling a reaction pathway for the dehydrogenative C–C coupling of the HAT molecules. Upon thermal treatment of co-deposited HAT and NaCl sub-monolayers on Ag surfaces, the ionic lattice decomposes (see XPS data in Figure S2), with Cl⁻ desorbing in form of volatile AgCl species,[27] while part of the Na remains on the surface.[28] This suggests a potential role of the Na adatoms in driving the polymerization. Spontaneous dissociation of NaCl and subsequent coordination of Na adatoms with organic molecules have been reported to occur upon surface annealing at elevated temperatures.[28–32] However, apart from simple intramolecular reactions such as tautomeric isomerization of guanine[33] and deprotonation of terephthalic acid,[34] no Na-assisted intermolecular coupling has been identified so far.

Detailed insight is provided by AFM imaging with CO-functionalized tips.[35] The contrast in the AFM frequency shift (Δf) image (Figure 2b) clarifies the formation of covalent bonds between the HAT molecules, whereby the activation of the hydrogen atoms in *meta*-positions to the chelating N atoms leads to covalently bonded linear structures (Figure 2b). Notably, each chain is coupled with a parallel one, indicating the presence of atomic species which coordinate to adjacent chelating N^N pockets. However, likely due to the lower adsorption height with respect to the molecular structures, they cannot be resolved by constant-height AFM imaging.[36,37] Since both Na and Ag adatoms could potentially coordinate with the HAT molecules, chemical identification of the atomic species is crucial. Upon deposition of the HAT molecules on the bare Ag(111) and

annealing to 300 K, high-resolution AFM imaging revealed the formation of purely H-bonded structures, without any evidence of organometallic structures involving Ag adatoms.[24] This evidence suggests that coordination of the HAT molecules with Ag adatoms is not favorable, even at rather elevated temperatures where native surface adatoms become largely available,[38] indicating the incorporation of Na adatoms in the chelating N^N pockets. This scenario is also supported by the simulated constant-height AFM image[39] in Figure 2c, obtained using fully relaxed atomic structure of HAT polymer coordinated by Na on the Ag(111) surface (Figure 2d).

We performed quantum mechanical calculations to elucidate a possible reaction mechanism and regioselectivity of HAT molecules towards one-dimensional polymers. Namely we studied first the role of Na adatoms in the formation of the chain. Therefore, to understand the importance of Na, we carried out a comparative study of the interaction of Na and Ag adatoms with the monomer and dimer of HAT molecules on the Ag(111) surface. While the calculated Hirshfeld charge of a Ag adatom ($+0.04$ e) is negligible, showing its neutral character, the Na adatom has a notable positive charge ($+0.35$ e). This indicates a cationic character of sodium adatoms on the surface (see Table S1). The calculated binding energies of Na and Ag adatoms to HAT molecules show greater binding energy with the former for both monomer and dimer complexes (see Table S2). This demonstrates that an organometallic dimer formed by two HAT molecules with a Na adatom in between is the most stable system. Figure 3 displays the calculated differential electron density ($\Delta\rho$), defined as $\Delta\rho = \rho_{all}-\rho_{complex}-\rho_{Ag(111)}$, being ρ_{all}, $\rho_{complex}$ and $\rho_{Ag(111)}$, the electron
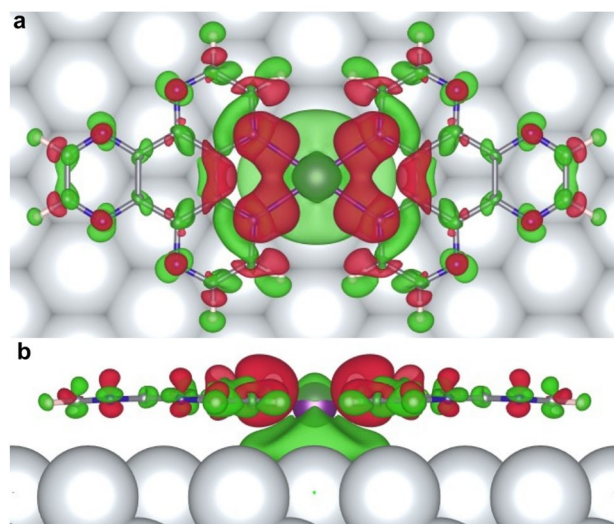

Figure 3. Calculated charge transfer between the (HAT)₂-Na complex and the Ag(111) surface. The differential electron density ($\Delta\rho$) is displayed at an isosurface of 0.005 e Å⁻³. Green and red colors represent negative and positive values of $\Delta\rho$, respectively. The spatial distribution of $\Delta\rho$ indicates strong interactions between the (HAT)₂-Na complex and Ag(111) via a pronounced charge transfer from the HAT ligands to the Ag(111). a, b) Top and side views, respectively.

densities of the relaxed complex on the surface, of the complex in the gas phase, and of the bare Ag(111) surface, respectively. The spatial distribution of $\Delta\rho$ indicates the presence of coordination bonds between Na and N atoms of HAT molecules (see also Figure S3). The total energy DFT calculations of the dimer (HAT)$_2$-Na complex on the Ag(111) surface reveal strong interactions between them, as corroborated by a pronounced charge transfer from HAT ligands to the substrate, which enhances the binding energy (see Table S2) of the dimer on the Ag(111) substrate. Notably, the formation of the (HAT)$_2$-Na complex substantially increases the desorption temperature with respect to bare HAT molecules, allowing for higher reaction temperatures to be reached before desorption from the surface. Thus, sodium complexation enables to reach elevated annealing temperatures facilitating the condition for polymerization reaction.

It is evident that the polymerization has to be initiated through removal of hydrogen atoms to form a free radical which will facilitate intermolecular covalent coupling between HAT units. Therefore, we first analyzed the bond-dissociation energies (BDE) for three inequivalent hydrogens presented in the monomer (HAT)$_1$-Na and dimer (HAT)$_2$-Na complexes, as shown in Figure 4a, b. Calculated values of BDE indicate a preferential hydrogen removal near the Na adatom. These BDE values in both cases (95.6 kcal mol^{-1} for the monomer and 92.4 kcal mol^{-1} for the dimer) are lower than a calculated BDE value for a free HAT molecule (112.2 kcal mol^{-1}) although still too high for temperature-driven direct C–H bond scission. Thus, we considered the possibility that the C–H bond breaking is mediated by an Ag adatom acting as a catalyst. In fact, such mobile adatoms, commonly present on metal surfaces at elevated temperatures, have been recently shown to promote important reaction steps, as keto-enol tautomeric dehydrogenation,[40] and C–C coupling.[41–43] Therefore, we carried out QM/MM[44] free energy calculations with WHAM methodology[45] to explore this hypothesis. Indeed, the QM/MM simulations reveal significant reduction of activation energies by ≈ 60 kcal mol^{-1}. We found that the lowest activation energy barrier of the dehydrogenation corresponds to *meta* position, 35.4 kcal mol^{-1}, for a molecule dimer (green in Figure 4c, d). The activation energies for the *ortho* (blue in Figure 4c, d) and *para* (red in Figure 4c, d) are slightly higher, being 41.9 and 50.2 kcal mol^{-1} respectively. It is between the dimer (HAT)$_2$-Na and the monomer (HAT)$_1$-Na (55 kcal mol^{-1}, Figure S4) where we observe that the dimer is not only the most stable structure, but also has a lower activation energy by 20 kcal mol^{-1}. These results point toward kinetically driven regioselectivity with a propensity of the system toward polymerization in the direction perpendicular to the (HAT)$_2$-Na complex, creating two parallel 1D chains held together by Na in tetradentate N^N position. It is worth emphasizing that the hydrogen removal in Figure 4 is only the first reaction step toward the polymer. The resulting (HAT)$_2$-Na radical complex is highly susceptible to the formation of covalently bonded complexes with adjacent (HAT)$_2$-Na radical rather than HAT itself, due to the energetic preference of the H- removal at their

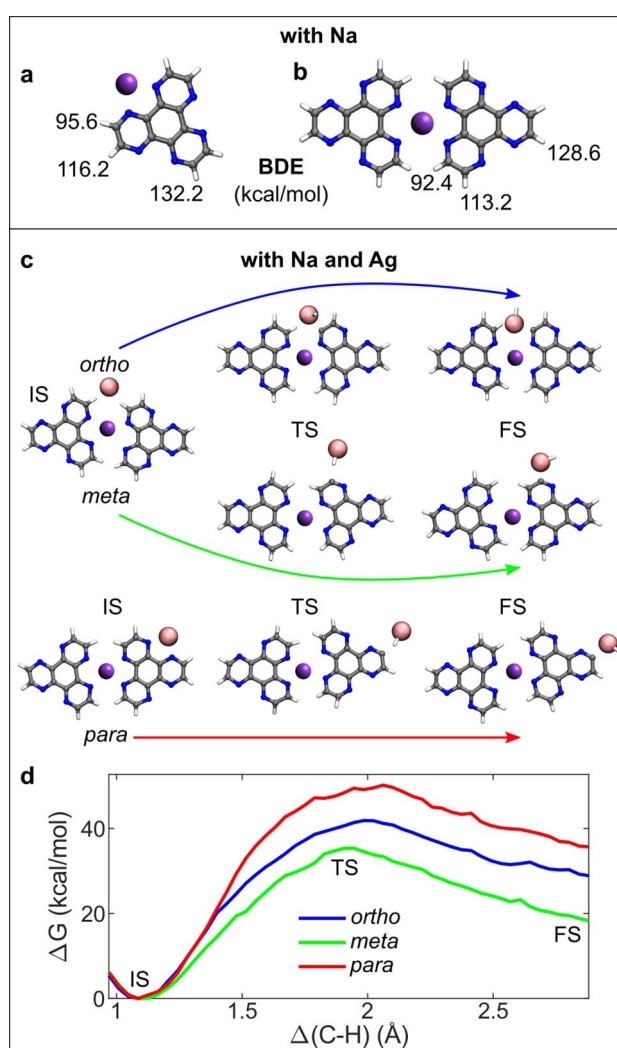**Figure 4.** HAT-Na complexes: (HAT)$_1$-Na (a) and (HAT)$_2$-Na (b). Bond-dissociation energies (BDE) for three inequivalent hydrogens are shown. Cooperative role of Na and Ag (c, d). Reaction pathways for the hydrogen removal in *ortho*, *meta* and *para* configurations (c). Corresponding free energy calculations as a function of the C–H distance (Δ) of the activated bond (d). Initial (IS), transition (TS), and final (FS) states are indicated (c, d).

meta positions. Therefore, we can assume that growth of linear polymeric structures occurs via coupling of (HAT)$_2$-Na complexes, rather than through the attachment of individual HAT radicals. This scenario is supported by the experimental observation of polymers composed of two chains of equal length, suggesting that the polymers grow directly as coupled chains, rather than by chain pairing upon cooling.

In conclusion, we investigated the on-surface polymerization of HAT molecules on Ag(111) in the presence of Na adatoms, leading to the formation of one-dimensional structures composed of coupled polymeric chains. By combining high-resolution scanning probe microscopy with DFT calculations, we elucidated the peculiar cooperative catalytic role of Na and Ag adatoms in steering both the polymerization and the regioselectivity of the Scholl reac-

Angew. Chem. Int. Ed. **2022**, *61*, e202112798 (4 of 6)

© 2021 The Authors. Angewandte Chemie International Edition published by Wiley-VCH GmbH

tion. Our results pave the way to further studies on cooperative catalytic effects of metal adatoms in steering novel coupling reactions on surfaces.

Conflict of Interest

The authors declare no conflict of interest.

Keywords: Atomic force microscopy · Cooperative effects · On-surface synthesis · Scanning tunneling microscopy · Surface chemistry

[1] M. Grzybowski, K. Skonieczny, H. Butenschoen, D. T. Gryko, *Angew. Chem. Int. Ed.* **2013**, *52*, 9900–9930; *Angew. Chem.* **2013**, *125*, 10084–10115.
[2] A. A. Sarhan, C. Bolm, *Chem. Soc. Rev.* **2009**, *38*, 2730–2744.
[3] D. Myśliwiec, B. Donnio, P. J. Chmielewski, B. Heinrich, M. Stępień, *J. Am. Chem. Soc.* **2012**, *134*, 4822–4833.
[4] Y. Cao, X.-Y. Wang, J.-Y. Wang, J. Pei, *Synlett* **2014**, *25*, 313–323.
[5] A. Narita, X.-Y. Wang, X. Feng, K. Müllen, *Chem. Soc. Rev.* **2015**, *44*, 6616–6643.
[6] M. S. Little, S. G. Yeates, A. A. Alwattar, K. W. Heard, J. Raftery, A. C. Edwards, A. V. Parry, P. Quayle, *Eur. J. Org. Chem.* **2017**, 1694–1703.
[7] Y. Han, Z. Xue, G. Li, Y. Gu, Y. Ni, S. Dong, C. Chi, *Angew. Chem. Int. Ed.* **2020**, *59*, 9026–9031; *Angew. Chem.* **2020**, *132*, 9111–9116.
[8] M. Uryu, T. Hiraga, Y. Koga, Y. Saito, K. Murakami, K. Itami, *Angew. Chem. Int. Ed.* **2020**, *59*, 6551–6554; *Angew. Chem.* **2020**, *132*, 6613–6616.
[9] H. Ito, Y. Segawa, K. Murakami, K. Itami, *J. Am. Chem. Soc.* **2019**, *141*, 3–10.
[10] B. T. King, J. Kroulík, C. R. Robertson, P. Rempala, C. L. Hilton, J. D. Korinek, L. M. Gortari, *J. Org. Chem.* **2007**, *72*, 2279–2288.
[11] J. Cai, P. Ruffieux, R. Jaafar, M. Bieri, T. Braun, S. Blankenburg, M. Muoth, A. P. Seitsonen, M. Saleh, X. Feng, K. Müllen, R. Fasel, *Nature* **2010**, *466*, 470–473.
[12] L. Grill, S. Hecht, *Nat. Chem.* **2020**, *12*, 115–130.
[13] P. Ruffieux, S. Wang, B. Yang, C. Sánchez-Sánchez, J. Liu, T. Dienel, L. Talirz, P. Shinde, C. A. Pignedoli, D. Passerone, T. Dumslaff, X. Feng, K. Müllen, R. Fasel, *Nature* **2016**, *531*, 489–492.
[14] J. Liu, R. Berger, K. Müllen, X. Feng, *From Polyphenylenes to Nanographenes and Graphene Nanoribbons*, Springer, Heidelberg, **2017**, pp. 1–32.
[15] Q. Fan, J. M. Gottfried, J. Zhu, *Acc. Chem. Res.* **2015**, *48*, 2484–2494.
[16] S. Clair, D. G. de Oteyza, *Chem. Rev.* **2019**, *119*, 4717–4776.
[17] Q. Fan, S. Werner, J. Tschakert, D. Ebeling, A. Schirmeisen, G. Hilt, W. Hieringer, J. M. Gottfried, *J. Am. Chem. Soc.* **2018**, *140*, 7526–7532.
[18] Q. Sun, C. Zhang, H. Kong, Q. Tan, W. Xu, *Chem. Commun.* **2014**, *50*, 11825–11828.
[19] C.-X. Wang, Q. Jin, C.-H. Shu, X. Hua, Y.-T. Long, P.-N. Liu, *Chem. Commun.* **2017**, *53*, 6347–6350.
[20] N. Kocić, X. Liu, S. Chen, S. Decurtins, O. Krejčí, P. Jelínek, J. Repp, S. X. Liu, *J. Am. Chem. Soc.* **2016**, *138*, 5585–5593.
[21] K. Sonogashira, Y. Tohda, N. Hagihara, *Tetrahedron Lett.* **1975**, *16*, 4467–4470.
[22] Q. Bi, X. Huang, G. Yin, T. Chen, X. Du, J. Cai, J. Xu, Z. Liu, Y. Han, F. Huang, *ChemCatChem* **2019**, *11*, 1295–1302.
[23] G. M. Sammis, H. Danjo, E. N. Jacobsen, *J. Am. Chem. Soc.* **2004**, *126*, 9928–9929.
[24] L. L. Patera, X. Liu, N. Mosso, S. Decurtins, S.-X. Liu, J. Repp, *Angew. Chem. Int. Ed.* **2017**, *56*, 10786–10790; *Angew. Chem.* **2017**, *129*, 10926–10930.
[25] S. Freund, R. Pawlak, L. Moser, A. Hinaut, R. Steiner, N. Marinakis, E. C. Constable, E. Meyer, C. E. Housecroft, T. Glatzel, *ACS Omega* **2018**, *3*, 12851–12856.
[26] T. Meier, R. Pawlak, S. Kawai, Y. Geng, X. Liu, S. Decurtins, P. Hapala, A. Baratoff, S.-X. Liu, P. Jelínek, E. Meyer, T. Glatzel, *ACS Nano* **2017**, *11*, 8413–8420.
[27] M. Bowker, K. Waugh, *Surf. Sci.* **1983**, *134*, 639–664.
[28] C. Wäckerlin, C. Iacovita, D. Chylarecka, P. Fesser, T. A. Jung, N. Ballav, *Chem. Commun.* **2011**, *47*, 9146.
[29] T. K. Shimizu, J. Jung, H. Imada, Y. Kim, *Angew. Chem. Int. Ed.* **2014**, *53*, 13729–13733; *Angew. Chem.* **2014**, *126*, 13949–13953.
[30] K. Zhou, H. Liang, M. Wang, S. Xing, H. Ding, Y. Song, Y. Wang, Q. Xu, J.-H. He, J. Zhu, W. Zhao, Y. Ma, Z. Shi, *Nanoscale Adv.* **2020**, *2*, 2170–2176.
[31] J. Hieulle, D. Peyrot, Z. Jiang, F. Silly, *Chem. Commun.* **2015**, *51*, 13162–13165.
[32] C. Zhang, L. Wang, L. Xie, H. Kong, Q. Tan, L. Cai, Q. Sun, W. Xu, *ChemPhysChem* **2015**, *16*, 2099–2105.
[33] C. Zhang, L. Xie, L. Wang, H. Kong, Q. Tan, W. Xu, *J. Am. Chem. Soc.* **2015**, *137*, 11795–11800.
[34] D. Skomski, S. Abb, S. L. Tait, *J. Am. Chem. Soc.* **2012**, *134*, 14165–14171.
[35] L. Gross, F. Mohn, N. Moll, P. Liljeroth, G. Meyer, *Science* **2009**, *325*, 1110–1114.
[36] F. Queck, O. Krejčí, P. Scheuerer, F. Bolland, M. Otyepka, P. Jelínek, J. Repp, *J. Am. Chem. Soc.* **2018**, *140*, 12884–12889.
[37] L. L. Patera, Z. Zou, C. Dri, C. Africh, J. Repp, G. Comelli, *Phys. Chem. Chem. Phys.* **2017**, *19*, 24605–24612.
[38] Z. Yang, J. Gebhardt, T. A. Schaub, T. Sander, J. Schönamsgruber, H. Soni, A. Görling, M. Kivala, S. Maier, *Nanoscale* **2018**, *10*, 3769–3776.
[39] P. Hapala, G. Kichin, C. Wagner, F. S. Tautz, R. Temirov, P. Jelínek, *Phys. Rev. B* **2014**, *90*, 085421.

[40] H. Kong, C. Zhang, Q. Sun, X. Yu, L. Xie, L. Wang, L. Li, S. Hu, H. Ju, Y. He, J. Zhu, W. Xu, *ACS Nano* **2018**, *12*, 9033–9039.

[41] M. Fritton, D. A. Duncan, P. S. Deimel, A. Rastgoo-Lahrood, F. Allegretti, J. V. Barth, W. M. Heckl, J. Björk, M. Lackinger, *J. Am. Chem. Soc.* **2019**, *141*, 4824–4832.

[42] L. L. Patera, F. Bianchini, C. Africh, C. Dri, G. Soldano, M. M. Mariscal, M. Peressi, G. Comelli, *Science* **2018**, *359*, 1243–1246.

[43] B. de la Torre, A. Matěj, A. Sánchez-Grande, B. Cirera, B. Mallada, E. Rodríguez-Sánchez, J. Santos, J. I. Mendieta-Moreno, S. Edalatmanesh, K. Lauwaet, M. Otyepka, M. Medveď, Á. Buendía, R. Miranda, N. Martín, P. Jelínek, D. Écija, *Nat. Commun.* **2020**, *11*, 4567.

[44] J. I. Mendieta-Moreno, R. C. Walker, J. P. Lewis, P. Gómez-Puertas, J. Mendieta, J. Ortega, *J. Chem. Theory Comput.* **2014**, *10*, 2185–2193.

[45] S. Kumar, J. M. Rosenberg, D. Bouzida, R. H. Swendsen, P. A. Kollman, *J. Comput. Chem.* **1992**, *13*, 1011–1021.